Inorganic Chemistry

ARTICLE

pubs.acs.org/IC

P_2^{2-} and P^{3-} Units in the $[Rh_8P_9]^{\delta-}$ Polyanion of $La_4Rh_8P_9$

Ulrike Pfannenschmidt,[†] Dirk Johrendt,[§] Frederik Behrends,[‡] Hellmut Eckert,[‡] Matthias Eul,[†] and Rainer Pöttgen*[,†]

[†]Institut für Anorganische und Analytische Chemie and [‡]Institut für Physikalische Chemie, Universität Münster Corrensstrasse 36, 48149 Münster, Germany

[§]Department Chemie, Ludwig-Maximilians-Universität München, Butenandtstrasse 5-13, 81377 München, Germany

Supporting Information

ABSTRACT: The phosphide $La_4Rh_8P_9$ was synthesized from the elements in a bismuth flux. The structure was refined from single crystal diffractometer data: space group *Cmcm*, a = 1303.1(2), b = 1893.2(2), c = 576.70(6) pm, wR2 = 0.0277, 1380 F^2 values, 65 variables. The rhodium and phosphorus atoms build up a three-dimensional $[Rh_8P_9]$ polyanion which leaves larger cages for the three crystallographically independent lanthanum sites. The rhodium atoms have between four and six phosphorus neighbors at Rh−P distance ranging from 229 to 254 pm. Three of the four crystallographically independent phosphorus atoms are isolated (P^{3-} units), while the P4 atoms form dimers with double bond character (208 pm P−P). The P_2^{2-} diphosphenide units bond side-on to a Rh3 and end-on to four Rh5 atoms. ^{31}P magic angle spinning (MAS) NMR spectroscopy is able to resolve three of the four crystallographically distinct phosphorus sites. The doubly bonded phosphorus site P4 is characterized by an axially symmetric shielding tensor of moderate anisotropy $\Delta\sigma = \sigma_{33} - \sigma_{iso}$ = 257 ppm. Electronic band structure calculations prove the metallic character and reveal the significant difference between the isolated P^{3-} and the phosphorus atoms of the P_2^{2-} units. Magnetic susceptibility measurement reveals Pauli paramagnetism.

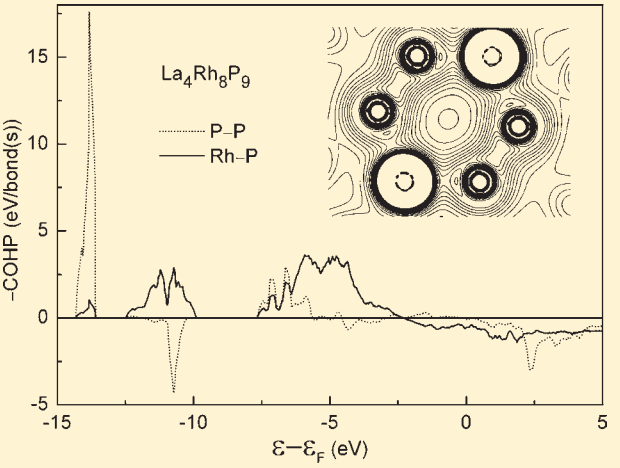

INTRODUCTION

The RET_2P_2 and AET_2P_2 phosphides (RE = rare earth element, AE = alkaline earth element, T = transition metal) mostly crystallize with the tetragonal $ThCr_2Si_2$ type structure, space group $I4/mmm$, a site occupancy variant of $BaAl_4$.[1,2] The tetrahedral $TP_{4/4}$ units in these phosphides are condensed via four common edges, and the resulting $[T_2P_2]$ layers are charge balanced and separated by the rare earth or alkaline earth cations. The interlayer P−P bonding strongly depends on the size of the rare earth or alkaline earth cation and the valence electron concentration. In the sequence $CaFe_2P_2 \rightarrow CaCo_2P_2 \rightarrow CaNi_2P_2 \rightarrow CaCu_{1.75}P_2$, the P−P distance decreases from 271 to 225 pm; i.e., one observes a transition from P^{3-} units to P−P single bond formation.[3−5]

These $ThCr_2Si_2$ type materials have attracted broad interest among solid state chemists and physicists since they exhibit highly interesting magnetic and electronic properties. Prominent examples are the heavy-fermion compound $CeCu_2Si_2$,[6] intermediate-valent $EuNi_2P_2$,[7] the incommensurate spiral antiferromagnet $EuCo_2P_2$,[8] or the recently reported charge density wave compound $BaFe_2As_2$,[9] which becomes superconducting upon Ba/K substitution.[10]

Besides the $ThCr_2Si_2$ type, some RET_2P_2 and AET_2P_2 phosphides crystallize with the $CaBe_2Ge_2$ or $CaAl_2Si_2$ type, which both show different connectivity of the $TP_{4/4}$ tetrahedra. Examples are the phosphides $RERh_2P_2$ (RE = La, Ce, Pr, Nd)[11] with $CaBe_2Ge_2$ type or $BaCd_2P_2$[12] with $CaAl_2Si_2$ type structure. A completely different structure has been observed for the isotypic phosphides $CaIr_2P_2$,[13] $SrIr_2P_2$, and $EuIr_2P_2$.[14] Here, part of the iridium and phosphorus atoms build up a three-dimensional network which includes the Ca (Sr, Eu) atoms and screw chains of the remaining iridium atoms. $BaPd_2P_2$[15] crystallizes with the tetragonal $CeMg_2Si_2$ type.

In several of the AE−T−P phase diagrams, one observes compounds with compositions very close to 1:2:2 but with different structural motifs. Examples are $Mg_4Rh_7P_6$ (i.e., $MgRh_{1.75}P_{1.5}$)[16] with $U_4Re_7Si_6$ and $Ca_4Ir_8P_7$ (i.e., $CaIr_2P_{1.75}$) with a new structure type.[17] During our recent studies on metal flux synthesis of metal-rich phosphides,[18,19] we accidentally obtained new phosphide $La_4Rh_8P_9$ (i.e., $LaRh_2P_{2.25}$) which has slightly higher phosphorus content than $CaBe_2Ge_2$ type $LaRh_2P_2$[11] but a different bonding pattern. The $[Rh_8P_9]$

Received: December 25, 2010
Published: February 25, 2011

polyanion of the $La_4Rh_8P_9$ structure contains isolated P^{3-} phosphide anions besides the rarely observed species of doubly bonded P_2^{2-} units. Herein, we report on the synthesis and structure determination of this new phosphide, its magnetic and bonding properties, and the differentiation of the crystallographically distinct phosphorus sites by ^{31}P solid state NMR spectroscopy.

Table 1. Crystal Data and Structure Refinement for $La_4Rh_8P_9$

Refined composition	$La_4Rh_8P_9$
Temperature	293 K
Formula mass (g mol^{-1})	1657.65
Space group	*Cmcm* (No. 63)
Formula units/cell, Z	4
Unit cell dimensions (pm)	a = 1303.1(2)
(Guinier Powder data)	b = 1893.2(2)
	c = 576.70(6)
Cell volume (nm^3)	V = 1.4227(3)
Calculated density (g cm^{-3})	7.74
Crystal dimensions (μm)	30 × 40 × 80
Range in 2θ	4−65°
Detector distance (mm)	80
Exposure time (min)	5
ω-range; $\Delta\omega$	0−180°; 1°
Integr. param. A, B, EMS	12.8; 2.9; 0.012
Transm. ratio (max/min)	0.703/0.445
Absorption coeff. (mm^{-1})	21.7
F(000)	2892
Range in *hkl*	±19, ± 28, ± 8
Total no. of reflections	8794
Independent reflections	1380 (R_{int} = 0.0367)
Reflections with $I > 2\sigma(I)$	1184 (R_{sigma} = 0.0277)
Data/parameter	1380/65
Goodness-of-fit on F^2	1.011
Final R indices	R1 = 0.0181
$[I > 2\sigma(I)]$	wR2 = 0.0268
Final R indices (all data)	R1 = 0.0267
	wR2 = 0.0279
Extinction parameter	0.00253(4)
Largest diff. peak/hole	1.17/−1.81 e Å^{-3}

EXPERIMENTAL SECTION

Synthesis. Starting materials for the preparation of $La_4Rh_8P_9$ were lanthanum filings (Heraeus, 99.9%), rhodium powder (Heraeus, >99.9%), red phosphorus (Hoechst, Knapsack, ultrapure), and bismuth granules (Chempur, 1−10 mm, >99.9%). The elements were mixed in the molar ratio 4:8:9:30 (La: Rh: P: Bi) and placed in an evacuated silica tube. The ampule was then heated in a muffle furnace to 770 K at a rate of 50 K/h and kept at that temperature for 24 h. Subsequently, the temperature was raised to 1370 K at the same rate. The sample was kept at 1370 K for 100 h and then slowly cooled to room temperature at a rate of 2 K/h. The excess bismuth flux was dissolved by a 1:1 molar mixture of H_2O_2 (ACROS 35%) and glacial acetic acid (VWR International). The resulting sample was washed with demineralized water. The reaction product consisted of pillar-shaped crystals of $La_4Rh_8P_9$ and platelet-like crystals of $LaRh_2P_2$. Crystals of $La_4Rh_8P_9$ were mechanically separated for the physical property measurements.

X-ray Powder Data. The purity of the powder sample was controlled by X-ray powder diffraction in a Guinier camera using Cu Kα_1 radiation (λ = 154.056 pm) and α-quartz (a = 491.30, c = 540.46 pm) as an internal standard. The Guinier camera was equipped with an image plate system (Fujifilm, BAS−1800). The orthorhombic lattice parameters were deduced from a least-squares refinement of the powder data. To ensure correct indexing, the experimental pattern was compared to a calculated one[20] using the positional parameters obtained from the structure refinement.

Single Crystal Data. A suitable single crystal of $La_4Rh_8P_9$ was glued to a small quartz fiber using bees wax and then examined on a Buerger precession camera (equipped with an image plate system, Fujifilm, BAS−1800) in order to establish the quality for intensity data collection. Single crystal intensity data were collected at room temperature by the use of a Stoe IPDS II diffractometer (graphite monochromated Mo Kα radiation) in oscillation mode. A numerical absorption correction was applied to the data set. All relevant crystallographic data and details of the data collection and evaluation are listed in Table 1.

EDX Analyses. The single crystal investigated on the diffractometer was studied by EDX using a Zeiss EVO MA10 scanning electron microscope with LaF_3, Rh, and GaP as standards for the semiquantitative measurements. The analyses at several points of the crystal of 20 ± 2 atom % La/38 ± 2 atom % Rh/42 ± 2 atom % P is close to the ideal composition of 19.0 atom % La/38.1 atom % Rh/42.9 atom % P. No

Table 2. Refined Atomic Positions and Displacement Parameters of $La_4Rh_8P_9$

Atom	Wyckoff Pos.	x	y	z	U_{11}	U_{22}	U_{33}	U_{23}	U_{13}	U_{12}	U_{eq}[a]
La1	4*c*	0	0.63951(2)	1/4	52(1)	55(2)	48(2)	0	0	0	52(1)
La2	8*g*	0.22449(2)	0.36485(1)	1/4	59(1)	53(1)	47(1)	0	0	−5(1)	53(1)
La3	4*c*	0	0.11059(2)	1/4	125(2)	92(2)	55(2)	0	0	0	91(1)
Rh1	8*e*	0.39431(2)	0	0	43(1)	66(1)	49(1)	2(1)	0	0	53(1)
Rh2	4*c*	0	0.29182(3)	1/4	42(2)	69(2)	48(2)	0	0	0	53(1)
Rh3	4*c*	0	0.81623(3)	1/4	58(2)	61(2)	52(2)	0	0	0	57(1)
Rh4	8*g*	0.25656(2)	0.19679(2)	1/4	49(1)	58(1)	56(2)	0	0	3(1)	54(1)
Rh5	8*e*	0.18096(2)	0	0	56(1)	67(2)	66(2)	4(1)	0	0	63(1)
P1	4*c*	0	0.42609(9)	1/4	53(6)	61(7)	49(7)	0	0	0	54(3)
P2	8*g*	0.28255(8)	0.07097(6)	1/4	62(4)	62(5)	52(5)	0	0	−5(4)	59(2)
P3	16*h*	0.37608(6)	0.25956(4)	0.0022(2)	61(3)	69(3)	55(3)	−2(3)	−2(3)	4(2)	61(1)
P4	8*g*	0.42006(8)	0.43639(6)	1/4	43(4)	78(5)	71(5)	0	0	3(4)	64(2)

[a] U_{eq} is defined as one-third of the derivative of the orthogonalized U_{ij}-tensor. The exponent of the anisotropic displacement parameters is defined through $\exp\{-2\pi^2 \cdot (U_{11}h^2a^{*2} + \ldots + U_{12}hka^*b^*)\}$.

dx.doi.org/10.1021/ic102570x |*Inorg. Chem.* 2011, 50, 3044–3051

Table 3. Interatomic Distances (pm) of $La_4Rh_8P_9$[a]

La1:	2	P2	311.6(1)	Rh4:	2	P3	240.53(9)
	4	P3	313.31(9)		1	P2	240.6(1)
	2	P1	313.96(8)		2	P3	242.49(9)
	2	Rh2	316.30(4)		2	La2	312.05(3)
	4	Rh1	330.92(4)		1	La2	320.91(5)
	1	Rh3	334.58(7)		1	La1	335.25(6)
	2	Rh4	335.25(5)	Rh5:	2	P4	229.39(9)
La2:	1	P4	288.6(1)		2	P2	237.41(9)
	2	P3	306.27(9)		1	Rh1	278.02(6)
	2	Rh4	312.05(3)		2	Rh5	288.35(3)
	2	P2	313.03(6)		2	La2	318.48(4)
	1	P1	314.67(8)		2	La3	346.74(4)
	2	P3	314.93(9)	P1:	4	Rh1	243.6(1)
	2	Rh5	318.48(4)		1	Rh2	254.2(2)
	1	Rh4	320.91(5)		2	La1	313.95(8)
	1	Rh2	323.56(5)		2	La2	314.67(8)
	2	Rh1	332.00(4)	P2:	2	Rh5	237.41(9)
	1	Rh3	370.63(6)		1	Rh4	240.6(1)
La3:	4	P4	319.23(5)		2	Rh1	245.1(1)
	2	Rh3	319.91(4)		1	La1	311.7(1)
	4	P3	328.12(9)		2	La2	313.03(6)
	1	Rh2	343.12(7)		1	P4	366.9(2)
	2	P4	345.9(1)		1	La3	375.8(1)
	4	Rh5	346.74(4)	P3:	1	Rh2	238.10(9)
	2	Rh4	372.03(6)		1	Rh4	240.53(9)
	2	P2	375.8(1)		1	Rh3	240.86(9)
Rh1:	2	P1	243.6(1)		1	Rh4	242.49(9)
	2	P2	245.1(1)		1	P3	285.8(2)
	1	Rh1	275.43(7)		1	P3	290.9(2)
	1	Rh5	278.02(6)		1	La2	306.28(9)
	2	Rh1	288.35(3)		1	La1	313.31(9)
	2	La1	330.92(4)		1	La2	314.93(9)
	2	La2	331.99(4)		1	P3	323.0(2)
Rh2:	4	P3	238.10(9)		1	La3	328.12(9)
	1	P1	254.2(2)	P4:	1	P4	208.3(2)
	2	La1	316.30(4)		2	Rh5	229.39(9)
	2	La2	323.56(5)		1	Rh3	250.2(1)
	1	La3	343.12(7)		1	La2	288.6(1)
Rh3:	4	P3	240.86(9)		2	La3	319.23(6)
	2	P4	250.2(1)		1	La3	345.9(1)
	2	La3	319.91(4)				
	1	La1	334.58(7)				

[a] All distances within the first coordination spheres are listed. Standard deviations are given in parentheses.

other impurity elements (especially bismuth incorporation from the flux) were observed.

Magnetic Data. Selected crystals (18.712 mg) of $La_4Rh_8P_9$ were packed in kapton foil and attached to the sample holder rod of a vibrating sample magnetometer (VSM) for measuring the magnetic properties in a quantum design physical-property-measurement system in the temperature range of 2.1−305 K with a magnetic flux density of 10 kOe.

^{31}P Solid State NMR. Solid state ^{31}P magic angle spinning (MAS) NMR data were obtained at 121.65 MHz on a Bruker DSX-300 NMR spectrometer operating with a 4 mm MAS NMR probe. Probe detuning effects caused by the metallic character of these samples were reduced by mixing them with quartz powder in a 1:1 mass ratio. Single-pulse excitation spectra were obtained with 90° pulses of 3 μs length at an MAS spinning frequency of 15 kHz, using a relaxation delay of 150 s. This delay was found to be sufficient for complete relaxation. MAS central lines and spinning sidebands were deconvoluted into individual Gaussian components using the TOPSPIN software. Chemical shifts are reported relative to 85% H_3PO_4 used as an external reference standard.

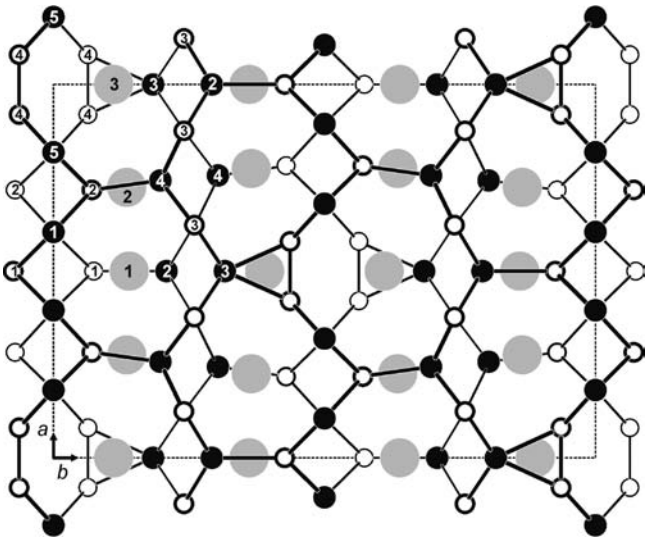

Figure 1. Projection of the $La_4Rh_8P_9$ structure along the *c* axis. Lanthanum, rhodium, and phosphorus atoms are drawn as medium gray, black filled, and open circles, respectively. The three-dimensional $[Rh_8P_9]$ polyanionic network and atom designations are emphasized.

Computational Details. Self-consistent density-functional theory (DFT) band structure calculations of $La_4Rh_8P_9$ were performed using the linear muffin-tin orbital (LMTO) method (program TB-LMTO-ASA)[21] in its scalar-relativistic version within the local density approximations (LDA) and atomic-sphere approximations (ASA). Complete space filling by the ASA spheres with a maximal overlap of 15% was achieved without additional empty spheres. Detailed descriptions are given elsewhere.[22] Reciprocal space integrations were performed with the tetrahedron method using 35 *k*-points within the irreducible wedge of the hexagonal Brillouin zone, which was divided in a 4 × 4 × 8 mesh. The basis set consisted of La:6s/{6p}/5d/4f, Rh:5s/5p/4d/{4f}, and P:3s/3p/{3d}. Orbitals given in parentheses were downfolded. The crystal orbital Hamilton population (COHP) method[23] was used for the bond analysis. COHP gives the energy contributions of all electronic states for a selected bond. The values are negative for bonding and positive for antibonding interactions. With respect to the crystal orbital overlap population (COOP) diagrams, we plot −COHP(E) to get positive values for bonding states.

RESULTS AND DISCUSSION

Structure Refinement. Systematic analyses of the $La_4Rh_8P_9$ data set revealed a *C*-centered orthorhombic lattice and the additional systematic extinctions *h*0*l* only observed for *h*, *l* = 2n, leading to the space groups *Cmcm*, *Cmc*2$_1$, and *C*2*cm* (*Ama*2), of which the centrosymmetric group was found to be correct during structure refinement. The starting atomic parameters were deduced from an interpretation of direct methods with SHELXS-97,[24] and the structure was refined using the SHELXL−97 code (full-matrix least-squares on F^2)[25] with anisotropic atomic displacement parameters for all atoms. As a

dx.doi.org/10.1021/ic102570x |*Inorg. Chem.* 2011, 50, 3044–3051

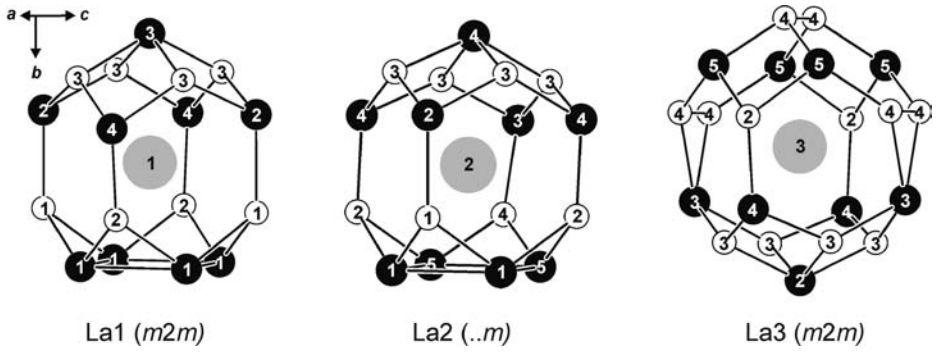

Figure 2. Coordination polyhedra of the lanthanum atoms in $La_4Rh_8P_9$. Lanthanum, rhodium, and phosphorus atoms are drawn as medium gray, black filled, and open circles, respectively. Atom designations and site symmetries are given.

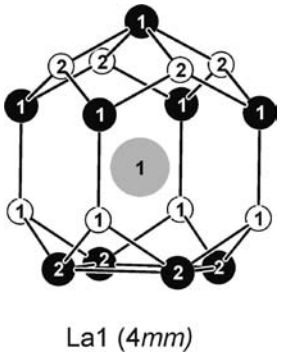

Figure 3. Coordination polyhedron of the lanthanum atoms in $LaRh_2P_2$. Lanthanum, rhodium, and phosphorus atoms are drawn as medium gray, black filled, and open circles, respectively. Atom designations and site symmetries are given.

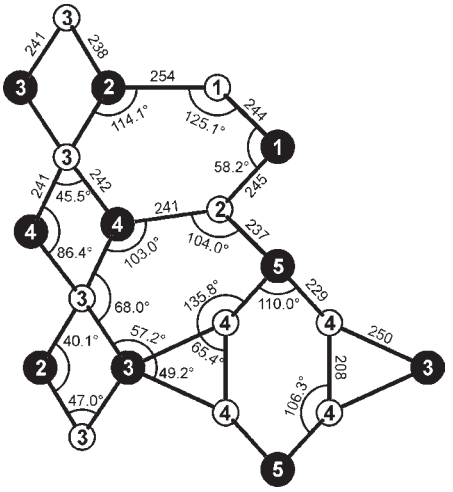

Figure 4. Cutout of the $[Rh_8P_9]^{\delta-}$ polyanion in $La_4Rh_8P_9$. Rhodium and phosphorus atoms are drawn as black filled and open circles, respectively. Atom designations as well as relevant interatomic distances and angles are indicated.

check for the correct composition, the occupancy parameters were refined in a separate series of least-squares cycles. All sites were fully occupied within less than two standard uncertainties, and in the final cycles, the ideal occupancy parameters were assumed again. A final difference electron-density map did not reveal any significant residual peaks. The results of the structure refinement are summarized in Table 1. The atomic coordinates and the interatomic distances are listed in Tables 2 and 3. Further information on the structure refinement is available from Fachinformationszentrum Karlsruhe, D-76344 Eggenstein-Leopoldshafen (Germany), by quoting the Registry No. CSD−422464.

Crystal Chemistry. Similar to the many metal-rich phosphides,[26] well-shaped crystals of the phosphide $La_4Rh_8P_9$ were also obtained from a metal flux. $La_4Rh_8P_9$ crystallizes with a new structure type. As emphasized in Figure 1, the rhodium and phosphorus atoms build up a complex three-dimensional $[Rh_8P_9]$ network which leaves larger cages for the lanthanum atoms. The coordination polyhedra of the lanthanum atoms are presented in Figure 2. La1 and La2 have coordination number (CN) 17 with 9 Rh and 8 P atoms in their coordination shell. These two coordination polyhedra resemble the $CaBe_2Ge_2$ type structure,[27] which, besides the $ThCr_2Si_2$ type, is another site occupancy variant of the $BaAl_4$ type.[28] As an example, we present the coordination polyhedron of $LaRh_2P_2$[11] in Figure 3. The latter phosphide crystallizes in space group $P4/nmm$ and the lanthanum atoms have site symmetry $4mm$. Within the matrix of the $La_4Rh_8P_9$ structure, the site symmetries of La1 and La2 reduce to $m2m$ and $..m$, respectively. Although the site symmetries are lowered, both structures have almost the same range of Rh−P distances (229−254 pm in $La_4Rh_8P_9$ and 234−249 pm in $LaRh_2P_2$) for the cages surrounding the lanthanum atoms. A similar situation occurs for the structure of $Ca_4Ir_8P_7$ (i.e., $CaIr_2P_{1.75}$),[17] where parts of the structure resemble the $ThCr_2Si_2$ type phosphide $CaRh_2P_2$.

The La3 atoms in $La_4Rh_8P_9$ show the much higher coordination number 21. Instead of eight single phosphorus neighbors, La3 is coordinated to six single phosphorus atoms and three P_2 units (Figure 2), leading to the enhanced coordination number. Again, also for La3, the lower part of the coordination polyhedron resembles the coordination in $LaRh_2P_2$[11] (Figure 3). The P_2 units coordinate side-on to the La3 atoms. Between the polyhedra, the shortest La−La distances are 411 pm, significantly longer than in *fcc* lanthanum (375 pm).[29] In view of the electropositive character of the lanthanum atoms (vide infra), we can safely rule out La−La interactions.

A cutout of the $[Rh_8P_9]$ network is presented in Figure 4. The Rh−P distances in the $La_4Rh_8P_9$ structure range from 229 to 254 pm, close to the sum of the covalent radii[30] of 235 pm. We can, therefore, assume substantial covalent Rh−P bonding within the $[Rh_8P_9]$ network. A similar range of Rh−P distances occurs in $CaBe_2Ge_2$ type $LaRh_2P_2$[11] with almost the same composition as

dx.doi.org/10.1021/ic102570x |*Inorg. Chem.* 2011, 50, 3044–3051

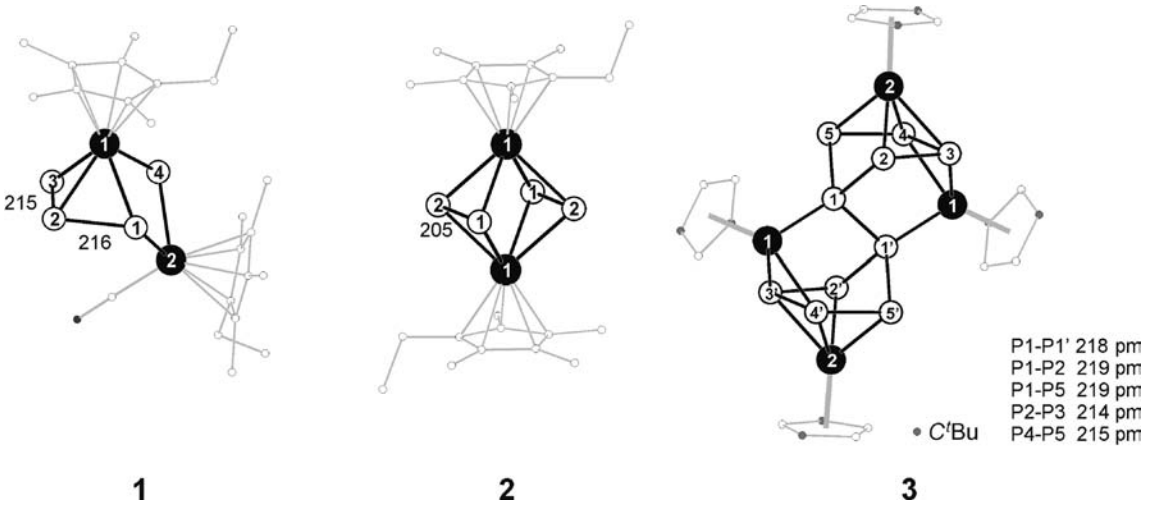

Figure 5. Rhodium−phosphorus substructures of $[(\eta^5\text{-}C_5Me_4Et)Rh\{(\eta^4\text{-}P_4Rh)(CO)(\eta^5\text{-}C_5Me_4Et)\}]$ (**1**),[34] $[(\eta^5\text{-}C_5Me_4Et)Rh(\mu,\eta^2\text{-}P_2)_2Rh(\eta^5\text{-}C_5Me_4Et)]$ (**2**),[36] and $[(Cp''Rh)_2(P_5{-}P_5)(RhCp'')_2]$, $Cp'' = C_5H_3(tBu)_2$ (**3**).[37] Rhodium and phosphorus atoms are drawn as black filled and open circles, respectively. Atom designations as well as relevant interatomic distances and angles are indicated.

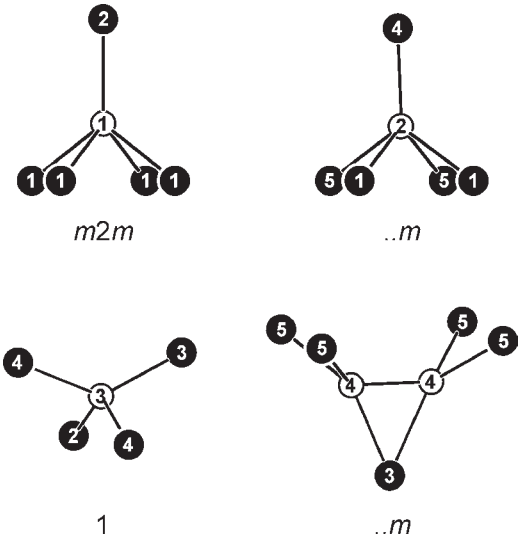

Figure 6. Rhodium coordination of the four crystallographically independent phosphorus sites in $La_4Rh_8P_9$. Atom designations and site symmetries are given.

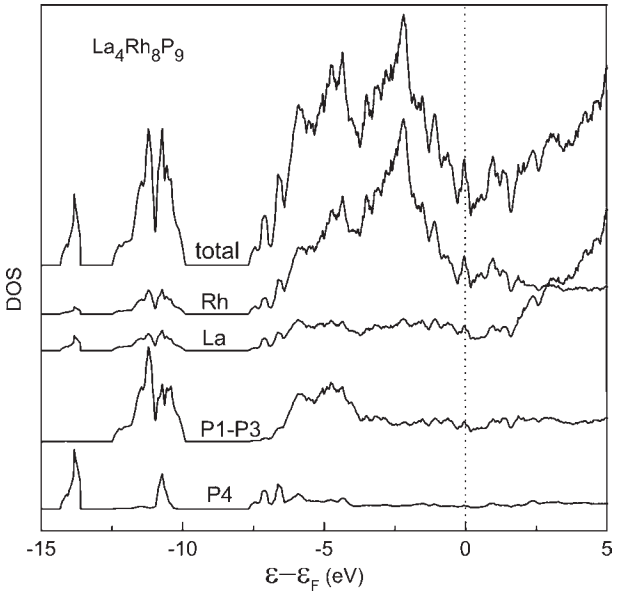

Figure 7. Total and partial density of states of $La_4Rh_8P_9$. The energy zero is taken at the Fermi level.

well as in $Mg_4Rh_7P_6$[16] (242−250 pm) with cubic $U_4Re_7Si_6$ type structure. A slightly broader range of Rh−P distances occurs in the complex structures of the metal-rich phosphides $Ca_5Rh_{19}P_{12}$ (228−275 pm),[31] $Ce_{12}Rh_{30}P_{21}$ (228−272 pm),[32] and $La_6Rh_{32}P_{17}$ (223−273 pm).[33] The rhodium atoms Rh1 and Rh5 have closer rhodium neighbors at Rh−Rh distances ranging from 275 to 288 pm, slightly longer than in *fcc* rhodium (268 pm),[29] and we can also assume some Rh−Rh bonding within the $[Rh_8P_9]$ network.

The phosphorus atoms P1, P2, and P3 within the $[Rh_8P_9]$ network have no nearest phosphorus neighbors and can, therefore, be considered as isolated P^{3-} units. This is different for the P4 atoms which have another P4 atom at 208 pm, much shorter than the average P−P single bond distance of 223 pm in diverse polyphosphides.[1] We can, therefore, assume P−P double bond character and formation of a P_2^{2-} unit. Thus, $La_4Rh_8P_9$ is the first ternary rare earth-transition metal phosphide with a P−P double bond. Within the structure, we observe side-on coordination of the P_2^{2-} unit to a Rh3 and end-on coordination to four Rh5 atoms (Figure 3).

Such units have previously been observed in coordination compounds with diverse P_x ligands. As examples, we present the rhodium−phosphorus skeletons of $[(\eta^5\text{-}C_5Me_4Et)Rh\{(\eta^4\text{-}P_4Rh)(CO)(\eta^5\text{-}C_5Me_4Et)\}]$ (**1**),[34] $[(\eta^5\text{-}C_5Me_4Et)Rh(\mu,\eta^2\text{-}P_2)_2Rh(\eta^5\text{-}C_5Me_4Et)]$ (**2**),[35] and $[(Cp''Rh)_2(P_5{-}P_5)(RhCp'')_2]$, $Cp'' = C_5H_3(tBu)_2$ (**3**)[36] in Figure 5. An overview of further complexes with other transition metals was given by Scherer.[37] In $[(\mu,\eta^2\text{-}P_2)Co_2(CO)_5(PPh_3)]$,[38] an even shorter P−P distance of 202 pm has been observed. The rhodium−phosphorus molecular units of these organometallic compounds are coordinated to different ligands, and the bonding situation certainly differs from that in the solid state phosphide $La_4Rh_8P_9$ (vide infra).

dx.doi.org/10.1021/ic102570x |*Inorg. Chem.* 2011, 50, 3044–3051

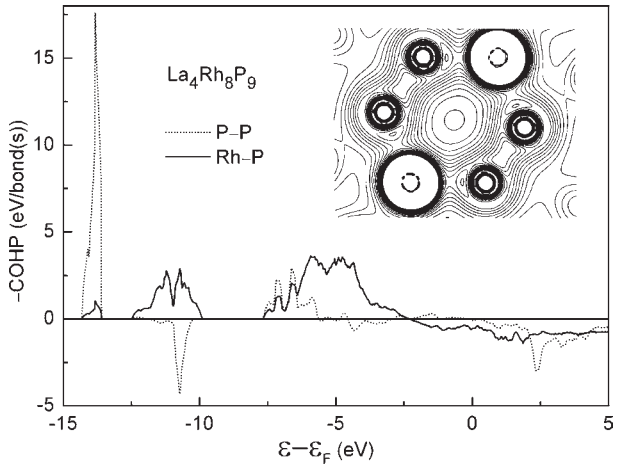

Figure 8. Crystal orbital Hamilton population (COHP) of the Rh−P (solid line) and *P*═P bonds (dashed line) in $La_4Rh_8P_9$. Inset: Valence electron density in the $Rh_2(P_2)_2$ six-membered ring as contour lines between 0 and 0.15 electrons/Å^3.

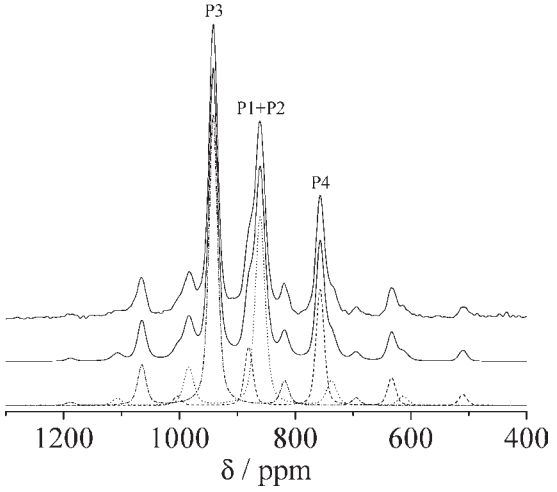

Figure 9. ^{31}P MAS NMR spectrum of $La_4Rh_8P_9$. Top trace: experimental data; middle trace: simulated spectrum; bottom trace: deconvolution into individual spinning sideband manifolds. Assignments of the central resonances to the crystallographically distinct phosphorus sites are indicated in the figure. All the other signals are magic angle spinning sidebands.

The rhodium coordination for the four crystallographically independent phosphorus sites in $La_4Rh_8P_9$ are presented in Figure 6. Note that the local environments of P1 and P2 are rather similar and distinctly different from those of P3 and P4, respectively.

Keeping the highly electropositive lanthanum atoms, the isolated P^{3-}, and P_2^{2-} units in mind, a $(4\ La^{3+})^{12+}(8\ Rh)^{11+}(7\ P^{3-})^{21-}(P_2)^{2-}$ ionic formula splitting in a first approximation. In order to evaluate this peculiar bonding situation within the $[Rh_8P_9]$ network of $La_4Rh_8P_9$ in more detail, we performed electronic structure calculations and further characterized $La_4Rh_8P_9$ by ^{31}P solid state NMR spectroscopy.

Electronic Structure of $La_4Rh_8P_9$. Figure 7 shows the total density of states (DOS) and projections of the Rh, La, and P contributions. In agreement with the magnetic susceptibility data (vide infra), $La_4Rh_8P_9$ proves to be a metal. The DOS at the

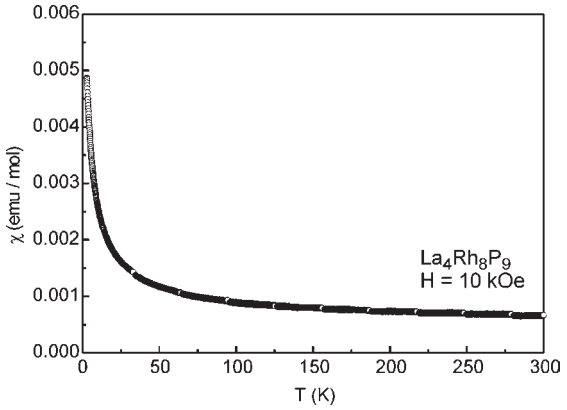

Figure 10. Temperature dependence of the magnetic susceptibility of $La_4Rh_8P_9$ measured at a field strength of 10 kOe.

Fermi-level roughly consists of 52% Rh-4*d*, 26% La-5*d*, and 22% P-3*s*,*p* states. The partial DOS of the isolated phosphorus-atoms (P1−P3) are similar and summed up in Figure 7. On the other hand, the partial DOS of the P4 atom is very different. We observe a considerably larger splitting of the 3*s* bands at −13 and −11 eV, resulting from the strong P═P bond. The latter is consistent with the bond analysis by the COHP method, shown in Figure 8. Contributions of the Rh−P bonds inside the RhP_n polyhedra (n = 4−6) are summed up for better comparison with the strong P═P bond. The large peak at −13 eV yields most of the P═P bonding energy, slightly reduced by its antibonding counterpart at −11 eV. The Rh−P bonding states around −5 and −12 eV are fully occupied and reveal the strong covalent mixing of P-*s*,*p* and Rh-*d* orbitals. Integrations of the COHP up to the Fermi level (ICOHP) yield an averaged Rh−P bonding energy of 2.5 eV/bond and a P═P bonding energy of 4.8 eV/bond, emphasizing the double bond character. In order to illustrate the bonding situation, we have calculated the valence electron density in the $Rh_2(P_2)_2$ six-membered ring plane, shown in Figure 8. The distinct accumulation of the electron density between the phosphorus atoms is obvious, and also, the polar Rh−P bonds are clearly visible.

^{31}P Solid State NMR. Figure 9 shows the solid state ^{31}P MAS NMR spectrum and its deconvolution into Gaussian components. Three spinning sideband manifolds are observed, which are centered at 942, 861, and 757 ppm, respectively. The area ratio of these peaks (including their associated spinning sidebands) is measured to be 3.6:3:2, which is close to a ratio of 4:3:2 expected from the crystal structure (Table 2), if the resonances of P1 and P2 are not resolved into individually distinct resonances. This result is consistent with Figure 6 and Table 2, indicating that the five-coordinated P1 and P2 sites have rather similar local environments. In contrast, the P3 site is four-coordinated with Rh and characterized by relatively short P···P distances in the second coordination sphere. On the basis of the site populations listed in Table 2, we assign the signal centered at 942 ppm to P3, the signal centered at 861 ppm to P1 and P2, and the signal centered at 757 ppm to P4. In addition, the chemical shift anisotropy defined as $\Delta\sigma = \sigma_{33} - \sigma_{iso}$ was analyzed from the spinning sideband intensity profiles using the DMFIT software.[39] We obtained $\Delta\sigma$ = 148, 185, and 259 ppm for P3, P1 and P2, and P4, respectively (cf. Figure 6). The asymmetry parameters are all found close to zero within experimental error. Not unexpectedly, the P4 site, having the short P−P bond length,

dx.doi.org/10.1021/ic102570x |*Inorg. Chem.* 2011, 50, 3044–3051

is characterized by a chemical shielding anisotropy that is significantly larger compared to those of the other phosphorus sites, all of which are regular P^{3-} species in distorted environments. Nevertheless, the chemical shift anisotropy found for this P=P double bond is significantly smaller than the value $\Delta\sigma = \sigma_{33} - \sigma_{iso}$ of 742 ppm previously measured for the compound 1,2-bis(2,4,6-tritert.butylphenyl)diphosphene.[40] This difference must be attributed to the significantly different bonding character of the present inorganic P_2^{2-} species from that in organophosphorus compounds.

Magnetic Susceptibility Data. The temperature dependence of the magnetic susceptibility of $La_4Rh_8P_9$ is shown in Figure 10. Over the entire temperature range, we observe very low susceptibility values with an almost temperature independent behavior between 100 and 300 K. At room temperature, we observe a susceptibility of $6.5(1) \times 10^{-4}$ emu/mol. This is a typical value of a Pauli paramagnet. The small upturn toward low temperature is attributed to traces of paramagnetic impurities. A measurement at 100 Oe down to 2 K gave no hint for a superconducting transition.

CONCLUSIONS

The new phosphide $La_4Rh_8P_9$ was synthesized in a bismuth flux. $La_4Rh_8P_9$ is metallic and a Pauli paramagnet. The $La_4Rh_8P_9$ structure is built up from a complex tree-dimensional $[Rh_8P_9]$ network which exhibits isolated P^{3-} besides double-bonded P_2^{2-} units, a new structural motif in the family of rare earth phosphides. The crystallographically different phosphorus units were resolved in ^{31}P solid state NMR spectra, and the P=P double bond character was manifested by electronic structure calculations.

ASSOCIATED CONTENT

Supporting Information. Crystallographic data in CIF format. This material is available free of charge via the Internet at http://pubs.acs.org.

AUTHOR INFORMATION

Corresponding Author
*E-mail: pottgen@uni-muenster.de.

ACKNOWLEDGMENT

We thank Dipl.-Chem. F. Tappe for the work at the scanning electron microscope, Dipl.-Ing. U. Ch. Rodewald for the intensity data collection, and Dr. J. J. Weigand for fruitful discussions. This work was supported by the Deutsche Forschungsgemeinschaft through SPP 1458 *Hochtemperatursupraleitung in Eisenpnictiden*. F.B. thanks the Fonds der Chemischen Industrie for a doctoral fellowship.

REFERENCES

(1) Villars, P.; Calvert, L. D. *Pearson's Handbook of Crystallographic Data for Intermetallic Compounds*; ASM International: Metals Park, Ohio, 1997 (Desk ed.) and 1991 (2nd ed.).
(2) Pöttgen, R.; Hönle, W.; von Schnering, H. G. In *Encyclopedia of Inorganic Chemistry*, 2nd ed.; King, R. B., Ed. Wiley: New York, 2005; Vol. VII, pp 4255−4308.
(3) Hoffmann, R.; Chong, Z. *J. Phys. Chem.* **1985**, *89*, 4175–4181.
(4) Zheng, C.; Hoffmann, R. *J. Solid State Chem.* **1988**, *72*, 58–71.
(5) Johrendt, D.; Felser, C.; Jepsen, O.; Andersen, O. K.; Mewis, A.; Rouxel, J. *J. Solid State Chem.* **1997**, *130*, 254–265.
(6) Steglich, F.; Aarts, J.; Bredl, C. D.; Lieke, W.; Meschede, D.; Franz, W.; Schäfer, H. *Phys. Rev. Lett.* **1979**, *43*, 1892–1896.
(7) Nagarajan, R.; Sampathkumaran, E. V.; Gupta, L. C.; Vijayaraghavan, R.; Prabhawalkar, V.; Bhaktdarshan; Padalia, B. D. *Phys. Lett.* **1981**, *84A*, 275–277.
(8) Reehuis, M.; Jeitschko, W.; Möller, M. H.; Brown, P. J. *J. Phys. Chem. Solids* **1992**, *53*, 987–690.
(9) Rotter, M.; Tegel, M.; Johrendt, D.; Schellenberg, I.; Hermes, W.; Pöttgen, R. *Phys. Rev. B* **2008**, *78*, 020503 (4 pp).
(10) Rotter, M.; Tegel, M.; Johrendt, D. *Phys. Rev. Lett.* **2008**, *101*, 107006 (4 pp).
(11) Madar, R.; Chaudouet, P.; Senateur, J. P.; Zemni, S.; Tranqui, D. *J. Less-Common Met.* **1987**, *133*, 303–311.
(12) Klüfers, P.; Mewis, A. *Z. Kristallogr.* **1984**, *169*, 135–147.
(13) Löhken, A.; Lux, C.; Johrendt, D.; Mewis, A. *Z. Anorg. Allg. Chem.* **2002**, *628*, 1472–1476.
(14) Lux, C.; Mewis, A.; Junk, S.; Gruetz, A.; Michels, G. *J. Alloys Compd.* **1993**, *200*, 135–139.
(15) Mewis, A. *Z. Naturforsch.* **1984**, *39b*, 713–720.
(16) Wurth, A.; Löhken, A.; Mewis, A. *Z. Anorg. Allg. Chem.* **2001**, *627*, 1213–1216.
(17) Löhken, A.; Mewis, A. *Z. Anorg. Allg. Chem.* **2004**, *630*, 2418–2421.
(18) Pfannenschmidt, U.; Rodewald, U. Ch.; Pöttgen, R. *Z. Anorg. Allg. Chem.* **2010**, *636*, 314–319.
(19) Pfannenschmidt, U.; Rodewald, U. Ch.; Pöttgen, R. *Z. Kristallogr.* **2010**, *225*, 280–286.
(20) Yvon, K.; Jeitschko, W.; Parthé, E. *J. Appl. Crystallogr.* **1977**, *10*, 73–74.
(21) Andersen, O. K.; Jepsen, O. Tight-Binding LMTO, Vers. 47c; Max-Planck-Institut für Festkörperforschung: Stuttgart, 1994.
(22) Andersen, O. K.; Jepsen, O.; Sob, M. In *Electronic Band Structure and its Applications, Lecture Notes in Physics*; Yussouff, M., Ed.; Springer Verlag: Berlin, 1987; Vol. 283, pp 1−57.
(23) Dronskowski, R.; Blöchl, P. E. *J. Phys. Chem.* **1993**, *97*, 8617–24.
(24) Sheldrick, G. M. SHELXS-97, Program for the Solution of Crystal Structures; University of Göttingen, Germany, 1997.
(25) (a) Sheldrick, G. M. SHELXL-97, Program for Crystal Structure Refinement; University of Göttingen, Germany, 1997. (b) Sheldrick, G. M. *Acta Crystallogr.* **2008**, *A64*, 112–122.
(26) Kanatzidis, M. G.; Pöttgen, R.; Jeitschko, W. *Angew. Chem., Int. Ed.* **2005**, *44*, 6996–7023.
(27) Eisenmann, B.; May, N.; Müller, W.; Schäfer, H. *Z. Naturforsch.* **1972**, *27b*, 1155–1157.
(28) Kussmann, D.; Pöttgen, R.; Rodewald, U. Ch.; Rosenhahn, C.; Mosel, B. D.; Kotzyba, G.; Künnen, B. *Z. Naturforsch.* **1999**, *54b*, 1155–1164.
(29) Donohue, J. *The Structures of the Elements*; Wiley: New York, 1974.
(30) Emsley, J. *The Elements*, Clarendon Press: Oxford, 1989.
(31) Wurth, A.; Löhken, A.; Mewis, A. *Z. Anorg. Allg. Chem.* **2002**, *628*, 661–666.
(32) Pivan, J. Y.; Guérin, R. *J. Less-Common. Met.* **1986**, *120*, 247–254.
(33) Pivan, J.-Y.; Guérin, R.; Pena, O.; Padiou, J.; Sergent, M. *Mater. Res. Bull.* **1988**, *23*, 513–520.
(34) Scherer, O. J.; Swarowsky, M.; Swarowsky, H.; Wolmershäuser, G. *Angew. Chem.* **1988**, *100*, 738–739.
(35) Scherer, O. J.; Swarowsky, M.; Wolmershäuser, G. *Angew. Chem.* **1988**, *100*, 423–424.
(36) Scherer, O. J.; Höbel, B.; Wolmershäuser, G. *Angew. Chem.* **1992**, *104*, 1042–1043.
(37) Scherer, O. J. *Comm. Inorg. Chem.* **1987**, *6*, 1–22.
(38) Campana, C. F.; Vizi-Orosz, A.; Palyi, G.; Markó, L.; Dahl, L. F. *Inorg. Chem.* **1979**, *18*, 3054–3059.

(39) Massiot, D.; Fayon, F.; Capron, M.; King, I.; Le Calve, S.; Alonso, B.; Durand, J. O.; Bujoli, B.; Gan, Z.; Hoatson, G. *Magn. Reson. Chem.* **2002**, *40*, 70.
(40) Zilm, K. W.; Webb, G. G.; Cowley, A. H.; Pakulski, M.; Orendt, A. *J. Am. Chem. Soc.* **1988**, *110*, 2032.